Ensemble Inequivalence in Long-Range Quantum Systems

Nicolò Defenu*
Institute for Theoretical Physics, ETH Zürich, Wolfgang-Pauli-Strasse 27, 8093 Zürich, Switzerland

David Mukamel
Department of Physics of Complex Systems, Weizmann Institute of Science, Rehovot 7610001, Israel

Stefano Ruffo
SISSA and INFN Sezione di Trieste, Via Bonomea 265, I-34136 Trieste, Italy
and Istituto dei Sistemi Complessi, Consiglio Nazionale delle Ricerche,
Via Madonna del Piano 10, I-50019 Sesto Fiorentino, Italy

(Received 17 March 2024; accepted 26 June 2024; published 2 August 2024)

Ensemble inequivalence, i.e., the possibility of observing different thermodynamic properties depending on the statistical ensemble which describes the system, is one of the hallmarks of long-range physics, which has been demonstrated in numerous classical systems. Here, an example of ensemble inequivalence of a long-range *quantum* ferromagnet is presented. While the $T = 0$ microcanonical quantum phase-diagram coincides with that of the canonical ensemble, the phase diagrams of the two ensembles are different at finite temperature. This is in contrast with the common lore of statistical mechanics of systems with short-range interactions where thermodynamic properties are bound to coincide for macroscopic systems described by different ensembles. The consequences of these findings in the context of atomic, molecular, and optical setups are delineated.

DOI: 10.1103/PhysRevLett.133.050403

Introduction—In recent years the interest of the research community in the equilibrium and dynamical behavior of long-range interacting quantum systems has experienced a unprecedented surge. Part of this enthusiasm stems from recent developments in the control, manipulation, and observation of atomic, molecular, and optical (AMO) systems, where long-range interactions within the microscopic components of the system are prevalent [1–8]. Conventionally, we refer to a many-body system as long-ranged if its two-body interaction potential $V(r)$ decays as a power law of the distance r, $V(r) \propto r^{-\alpha}$, with sufficiently small and positive α.

The system's phenomenology is heavily influenced by the exponent α. For $\alpha > \alpha_*$, with α_* a universal threshold value, the critical behavior mirrors that of systems with short-range interactions, while for $d < \alpha < \alpha_*$ in d dimensions the universal scaling near the phase transition is modified by the long-range couplings [9–13]. In the strong long-range regime ($\alpha < d$), where traditional thermodynamics does not apply, rescaling the interaction strength by an appropriate size dependent factor, i.e., the Kac's rescaling, restores energy extensivity but leaves most thermodynamic functions nonadditive. Notably, it has been demonstrated in numerous classical systems that this regime exhibits the appearance of *quasi-stationary states* (QSSs) [14–17] and *ensemble inequivalence* [18], two of the hallmarks of long-range physics. QSSs are metastable configurations of the out-of-equilibrium dynamics, whose lifetimes diverge with the system size [14–16], while *ensemble inequivalence* results in differing properties across thermodynamic ensembles and is the focus of the present Letter.

The quantum statistical mechanics of strong long-range interacting systems is to a large extent unexplored with few notable exceptions, which have been identified following the classical physics chart. In fact, theoretical evidence on quantum QSSs [19–21], which recently found a unified explanation based on the quasi-particle spectrum in strong long-range systems [22], should be compared with ergodicity breaking in classical systems, which is especially relevant in the microcanonical ensemble [23,24]. Ensemble inequivalence has also been discussed in the context of the finite temperature transition of quantum mechanical models [25–27]. With the rise of quantum simulators featuring native long-range interactions [8], it has become crucial to understand the impact of this significant phenomenon in the vicinity of a quantum critical point.

In this Letter, a genuine example of quantum ensemble inequivalence is presented, where the canonical and microcanical phase diagrams are different. This is done by analyzing a quantum model with long-range fully connected interactions and multispin couplings, which is known to exhibit a $T = 0$ paramagnetic to ferromagnetic transition [28]. The transition line is composed of first-order and second-order segments separated by a tricritical

*Contact author: ndefenu@phys.ethz.ch

point. We show that, while the two ensembles yield the same $T = 0$ phase diagram, they result in different finite temperature phase diagrams.

The relevance of this study is particularly evident nowadays, as the AMO community is pushing the investigation of quantum many-body systems toward the control of multibody interactions [29,30], where quantum tricritical points naturally occur [31]. Interestingly, some experimental AMO settings [8] can be considered either as isolated microcanonical systems, such as ensembles of dipolar atoms and molecules [32–34], or as canonical systems in contact with a thermal bath, such as cold atoms in cavities [7]. The latter systems are particularly relevant to our study since the interactions mediated by the cavity photons are global and flat, providing the optimal platform to experimentally verify our findings [21,35–37]. In fact, cavity QED experiments were recently employed to investigate the peculiar pre-thermalization dynamics of long-range assemblies [38]. From a broader perspective, the realization of fully connected quantum Hamiltonians is also relevant to the optimization of classical combinatorial problems via adiabatic quantum computing [39].

The model—It is convenient to discuss our findings in a concrete example of long-range quantum system, where the extension of the classical picture to the quantum realm can be carried out explicitly. Therefore, we introduce the Hamiltonian of a long-range quantum ferromagnetic spin-1/2 chain with 4-spin interactions

$$\mathcal{H} = -\frac{J}{N}\left(\sum\nolimits_{\ell}\sigma_{\ell}^{z}\right)^{2} - h\sum_{\ell}\sigma_{\ell}^{x} - \frac{K}{N^{3}}\left(\sum\nolimits_{\ell}\sigma_{\ell}^{z}\right)^{4}, \tag{1}$$

where the summations are taken over all values of the index $\ell \in \{1, \ldots, N\}$ which labels the N sites of the lattice. The σ_{ℓ}^{μ} operators are the $\mu = x, y, z$ Pauli matrices at site ℓ

$$\sigma_{\ell}^{x} = \begin{pmatrix} 0 & 1 \\ 1 & 0 \end{pmatrix}, \quad \sigma_{\ell}^{y} = \begin{pmatrix} 0 & -i \\ i & 0 \end{pmatrix}, \quad \sigma_{\ell}^{z} = \begin{pmatrix} 1 & 0 \\ 0 & -1 \end{pmatrix}. \tag{2}$$

In the following, we restrict the discussion to the fully ferromagnetic case $J, K > 0$.

Let us define the vector operator

$$\mathbf{S} = \frac{1}{2}\sum_{\ell}\boldsymbol{\sigma}_{\ell}, \tag{3}$$

where we use the bold face vector notation $\mathbf{S} = (S^x, S^y, S^z)$ and similarly for $\boldsymbol{\sigma}$. In terms of this operator, the Hamiltonian takes the form

$$\mathcal{H} = -\frac{4J}{N}(S^z)^2 - 2hS^x - \frac{16K}{N^3}(S^z)^4. \tag{4}$$

The Hamiltonian in Eq. (1) reduces to the celebrated Lipkin-Meshkov-Glick (LMG) model in the $K \to 0$ limit [40–42]. There, the system is known to possess a $T = 0$ quantum critical point at $h = h_c = 2J$, where a phase transition occurs between a paramagnetic state, fully aligned along x, and a ferromagnetic state with a nonvanishing magnetization along z.

Models like in Eq. (1) have been used to study various physical systems in both canonical and microcanonical settings. In the canonical setting, the quantum critical point is closely related to the Dicke model [43], observable by coupling the motional degrees of freedom of a Bose gas with a cavity's standing wave-field [44,45]. The Dicke model can be mapped onto the LMG model [46], showing that the transition from a disordered atom cloud to a self-organized phase is a second-order phase transition in the same universality class as the Hamiltonian-Mean-Field model [16,47]. Spin Hamiltonians like Eq. (1) can also be realized by coupling the internal degrees of freedom of atoms with the cavity field [48–51]. In contrast, systems like coupled Bose-Einstein condensates (BECs), the Bose-Hubbard model in a double well potential [52], spin-1 BECs [53–58], or Rydberg atoms in the blockade regime [59–63] are better described in a microcanonical setting. Therefore, it would be of interest to study a model like Eq. (1) within both canonical and microcanonical settings.

An important aspect of model (1) is the inclusion of multi-spin interactions. In fact, previous studies have been limited to the Hamiltonian (1) in the $K \to 0$ limit. The study of model (1) fits well within the current experimental endeavours that are pushing toward the quantum control of multibody interactions [64,65]. Multispin interactions have also been applied to model order-disorder ferroelectric transitions [28].

Model analysis—Hamiltonian (1) commutes with the total spin operator

$$\mathbf{S}^2 = \left(\frac{1}{2}\sum\nolimits_{\ell}\boldsymbol{\sigma}_{\ell}\right)^{2}. \tag{5}$$

As a result, the Hilbert space decomposes into a set of subspaces, each with a fixed value of total spin $S = 0, \ldots, M$, with $M = N/2$, where for simplicity we restricted the lattice to have an even number of sites. The eigenvalue of the total spin operator in the S subspace is $S(S+1)$. One notes that one has $g(S)$ possible ways to arrange the microscopic 1/2 spins in order to form a total spin S, with [28]

$$g(S) = \binom{2M}{M+S} - \binom{2M}{M+S+1}. \tag{6}$$

This formula can be verified by observing that the number of states with $S^z = S$ is given by the first term on the right-hand side of Eq. (6). However, some of these states belong to higher total spin S sectors, whose number is given by the second term in the equation above.

We proceed by calculating the free energy and the entropy of the model. We thus define the partition function Z and the phase space volume Ω as

$$Z(\beta, J, h, K) = \mathrm{Tr}[e^{-\beta\mathcal{H}}], \tag{7}$$

$$\Omega(E,J,h,K)=\mathrm{Tr}[\delta(E-\mathcal{H})], \tag{8}$$

where $\delta(\cdots)$ is the Dirac δ function and $\beta=1/T$ is the inverse temperature. Using the Hilbert space decomposition and the degeneracy $g(S)$, the traces can be more explicitly expressed as

$$Z(\beta,J,h,K)=\sum_S g(S)\sum_{S^z=-S}^{S}\langle S,S^z|e^{-\beta\mathcal{H}}|S,S^z\rangle, \tag{9}$$

$$\Omega(E,J,h,K)=\sum_S g(S)\sum_{S^z=-S}^{S}\langle S,S^z|\delta(E-\mathcal{H})|S,S^z\rangle. \tag{10}$$

Because of the mean-field nature of the interaction, the summations in these formulas can be evaluated straightforwardly in the thermodynamic limit. Let us define $S=Ms$ and note that s becomes a continuous variable in the interval [0, 1] as $M\to\infty$. Moreover, the energy density is defined as $\varepsilon=E/N$. The magnetization can be written as a classical vector $\mathbf{S}=Ms\mathbf{m}$, where $\mathbf{m}\equiv(m_x,m_y,m_z)=(\sin\theta\cos\phi,\sin\theta\sin\phi,\cos\theta)$ is a unit vector representing the orientation of the magnetization and $s\mathbf{m}$ is the magnetization vector per spin. The sums can thus be replaced by integrals yielding [66,67]

$$Z(\beta,J,h,K)=\int_0^1 ds\frac{N(Ns+1)}{8\pi}g(Ms)\times\int e^{-N\beta e(s,\theta,\phi,J,h,K)}\sin\theta d\theta d\phi, \tag{11}$$

$$\Omega(\varepsilon,J,h,K)=\int_0^1 ds\frac{N(Ns+1)}{8\pi}g(Ms)\times\int\delta[E-Ne(s,\theta,\phi,J,h,K)]\sin\theta d\theta d\phi, \tag{12}$$

where

$$e(s,\theta,\phi,J,h,K)=-Js^2\cos^2\theta-Ks^4\cos^4\theta-hs\sin\theta\cos\phi. \tag{13}$$

In the thermodynamic limit one can approximate the $g(Ms)$ factor using Stirling formula, giving the entropy

$$\mathcal{S}(s)=\frac{\log(g(Ms))}{2M}\approx-\frac{1+s}{2}\log\left(\frac{1+s}{2}\right)-\frac{1-s}{2}\log\left(\frac{1-s}{2}\right). \tag{14}$$

The partition sum becomes

$$Z(\beta,J,h,K)=\int_0^1 ds\frac{N(Ns+1)}{8\pi}\times\int e^{-N\beta(e(s,\theta,\phi,J,h,K)-\mathcal{S}(s)/\beta)}\sin\theta d\theta d\phi. \tag{15}$$

The phase-space volume $\Omega(\varepsilon,J,h,K)$ can be calculated using the Fourier representation of the δ function yielding

$$\Omega(\varepsilon,J,h,K)=\int_{-\infty}^{+\infty}\frac{d\lambda}{2\pi}\int_0^1 ds\frac{N(Ns+1)}{8\pi}\times\int e^{-i\lambda N(\varepsilon-e(s,\theta,\phi,J,h,K)+\mathcal{S}(s)/\lambda)}\sin\theta d\theta d\phi. \tag{16}$$

As the thermodynamic limit is approached the integrals in Eqs. (15) and (16) are dominated by the saddle points of the arguments of the exponentials. In both cases, the value of ϕ is unambiguously fixed at $\phi=0$, leaving only one single free parameter in the canonical ensemble $m_z=\cos\theta\in[-1,1]$. On the other hand, the microcanonical ensemble also requires an additional extremization with respect to the parameter λ, which results in a constraint on the average energy of the system $\langle\hat{\mathcal{H}}\rangle=\varepsilon$. In what follows, we first consider the phase diagram in the ground state and then analyze the finite-temperature phase diagrams in the two ensembles.

Ground-state phase-diagram—Quantum critical behavior occurs at zero temperature $T=0$, where thermal fluctuations do not affect quantum coherence. In this limit, the system configuration matches the Hamiltonian's ground state, so both the canonical and microcanonical ensembles yield the same phase diagram. Considering non-negative parameters J, h, and K, the ground state of the model is always in the $s=1$ subset of the spectrum, as shown by the energy expression (13). One then needs to minimize the energy with respect to θ. Expressing the energy (13) in terms of $m_z\equiv\cos\theta$ and expanding it in powers of m_z, one obtains

$$\varepsilon(m_z,J,h,K)=-Jm_z^2-Km_z^4-h\sqrt{1-m_z^2}\approx-h+\left(\frac{h}{2}-J\right)m_z^2+\left(\frac{h}{8}-K\right)m_z^4+\frac{h}{16}m_z^6+O(m_z^8). \tag{17}$$

This energy yields a second order critical line at $h=h_c=2J$, separating a disordered state $m_z=0$ from and ordered one with nonvanishing m_z. This result is valid as long as the fourth-order term in the expansion of the energy is positive. The transition becomes first order when the fourth-order term changes sign at the tricritical point given by $h/J=2$ and $K/J=1/4$. Close to this point, the first-order transition is given by

$$\frac{K}{J}=\frac{h}{8J}+\frac{1}{2}\sqrt{\frac{h}{J}\frac{(h/J-2)}{2}}. \tag{18}$$

The complete ground-state phase diagram, shared by both the canonical and microcanonical ensembles, is given in Fig. 1. In the following, we calculate the phase diagram at finite temperature, where we find that the two ensembles yield different phase diagrams.

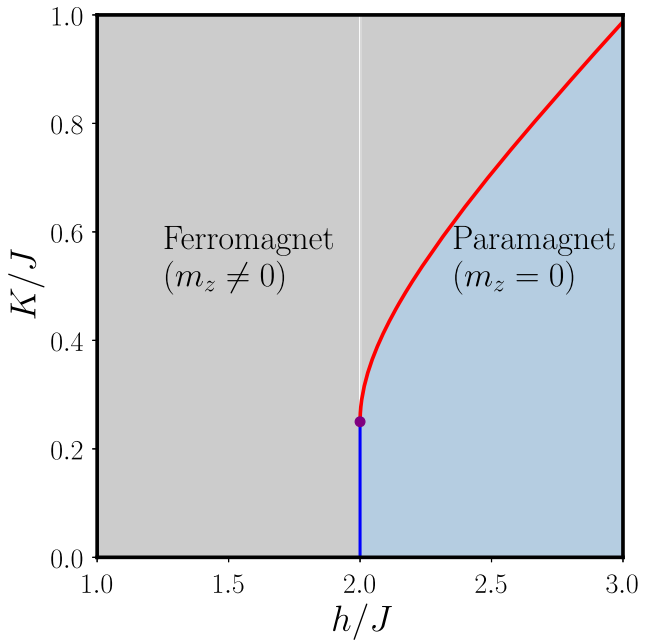

FIG. 1. The ground-state ($T = 0$) phase diagram of the model defined in Eq. (1) in the $(K/J, h/J)$ plane. It corresponds to both microcanonical and canonical ensembles. The phase-diagram displays a paramagnetic phase with $m_z = 0$ (blue shaded area) in the high h/J region. This phase is separated from the ferromagnetic phase where m_z is nonvanishing (gray shaded area) by a second order transition line at $h/J = 2$ for $K/J < 1/4$ (blue line). The transition becomes first-order (red line) at the tricritical point $(K/J = 1/4, h/J = 2)$. The first-order line is given in Eq. (18).

Phase-diagram in the canonical ensemble—Let us consider the free energy of the model

$$\begin{aligned} f(\beta, J, h, K) &= e - \mathcal{S}/\beta \\ &= -Js^2 m_z^2 - Ks^4 m_z^4 \\ &\quad - hs\sqrt{1 - m_z^2} + \frac{1}{\beta}\left[\frac{1+s}{2}\ln\frac{1+s}{2}\right. \\ &\quad \left. + \frac{1-s}{2}\ln\frac{1-s}{2}\right]. \end{aligned} \tag{19}$$

In order to find the equilibrium state of the system, one needs to minimize f with respect to s and m. Minimizing (19) with respect to s first, we obtain an expansion of s as a function of m_z,

$$s = s_0 + a m_z^2 + O(m_z^4), \tag{20}$$

where

$$s_0 = \tanh(\beta h), \tag{21a}$$

$$a = \beta(1 - s_0^2)\left(2Js_0 - \frac{h}{2}\right). \tag{21b}$$

Inserting the expansion (20) in the free energy (19), one obtains an expansion of f in powers of m_z^2:

$$f = f_0 + b_2 m_z^2 + b_4 m_z^4 + O(m_z^6), \tag{22}$$

with

$$f_0 = -hs_0 + \frac{1}{\beta}\mathcal{S}(s_0), \tag{23a}$$

$$b_2 = \frac{1}{2}hs_0 - Js_0^2. \tag{23b}$$

At criticality $b_2 = 0$, yielding

$$s_0 = \frac{h}{2J}, \tag{24}$$

and the critical line is given by

$$\frac{h}{2J} = \tanh\beta h, \tag{25}$$

as long as $b_4 > 0$. At low temperature the critical line is given, to leading order, by

$$\frac{h}{2J} \approx 1 - 2e^{-2\beta h}. \tag{26}$$

To proceed, we evaluate b_4 and locate the tricritical point at $b_2 = b_4 = 0$. We first expand the entropy in powers δs for $s = s_0 + \delta s$,

$$\mathcal{S}(s) \approx \mathcal{S}(s_0) + \frac{1}{2\beta}\ln\left(\frac{1+s_0}{1-s_0}\right)\delta s + \frac{1}{2\beta}\ln\left(\frac{1}{1-s_0^2}\right)\delta s^2. \tag{27}$$

Using this expansion with $\delta s = a m_z^2$, one finds that on the critical line $b_2 = 0$ the expression for b_4 is

$$b_4 = -\left(2Js_0 - \frac{1}{2}h\right)a - \left(Ks_0^4 - \frac{1}{8}hs_0\right) + \frac{1}{2\beta}\frac{1}{1-s_0^2}a^2. \tag{28}$$

Note that, due to the fact that $\partial f/\partial s|_{s_0} = 0$, higher order terms in the expansion (20) of s do not contribute to b_4. Using (21b) for a, we obtain

$$b_4 = -\left(Ks_0^4 - \frac{h}{8}s_0\right) - \frac{1}{8}\beta h^2(1 - s_0^2), \tag{29}$$

where at low temperature

$$s_0 = 1 - 2e^{-2\beta h}. \tag{30}$$

We finally arrive at the following expressions for the critical line ($b_2 = 0$) and the tricritical point ($b_2 = b_4 = 0$) in the canonical ensemble ([CE])

$$b_2 = 0\text{:}\ h_c[\mathrm{CE}] = 2J(1 - 2e^{-4\beta J}), \tag{31}$$

$$b_4 = 0\text{:}\ K_{tcp}[\mathrm{CE}] = \frac{J}{4} - 2\beta J^2 e^{-4\beta J}. \tag{32}$$

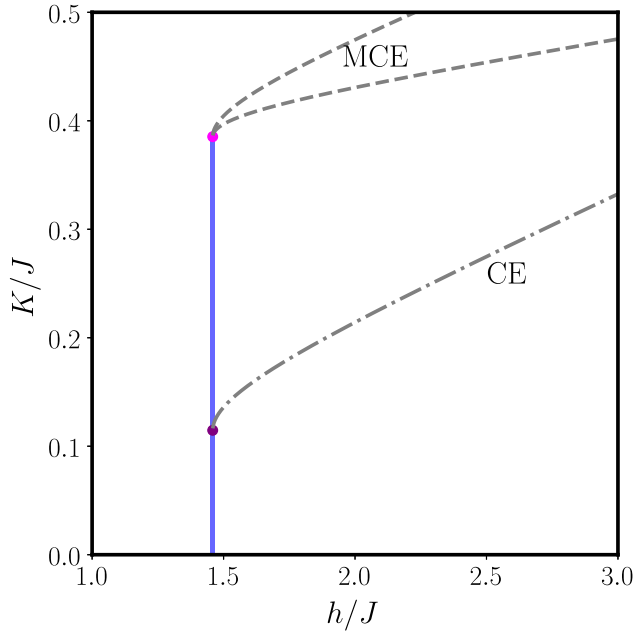

FIG. 2. The canonical and microcanonical $(h/J, K/J)$ phase diagrams at a given temperature ($\beta J = 1/2$). The microcanonical critical line coincides with the canonical one, but extends beyond the canonical tricritical point. While the critical line (blue) is drawn in scale, the first order lines (gray dashed lines in the microcanonical ensemble and a gray dot-dashed line in the canonical one) are only drawn schematically.

Phase-diagram in the microcanonical ensemble—The microcanonical phase-diagram can be readily obtained by minimizing the energy at constant entropy. The energy is given by

$$\varepsilon = -Js^2 m_z^2 - Ks^4 m_z^4 - hs\sqrt{1-m_z^2}$$
$$\approx -hs + \left(\frac{1}{2}hs - Js^2\right)m_z^2 + \left(\frac{1}{8}hs - Ks^4\right)m_z^4 + O(m_z^6). \tag{33}$$

The entropy $\mathcal{S}(s)$ (14) is a function of s only and thus one has to minimize the energy ε with respect to m_z at fixed s. The resulting critical line is

$$\frac{1}{2}hs - Js^2 = 0, \tag{34}$$

which, together with

$$\frac{1}{8}hs - Ks^4 = 0, \tag{35}$$

yields the tricritical point. To proceed, one has to express s in terms of the temperature. On the critical line, where $m_z = 0$, the energy is given by $\varepsilon = -hs$. Thus,

$$\beta = \frac{\partial \mathcal{S}}{\partial \varepsilon} = -\frac{1}{h}\frac{\partial \mathcal{S}}{\partial s} = \frac{1}{2h}\ln\frac{1-s}{1+s}, \tag{36}$$

which gives

$$s = \tanh \beta h \approx 1 - 2e^{-2\beta h}. \tag{37}$$

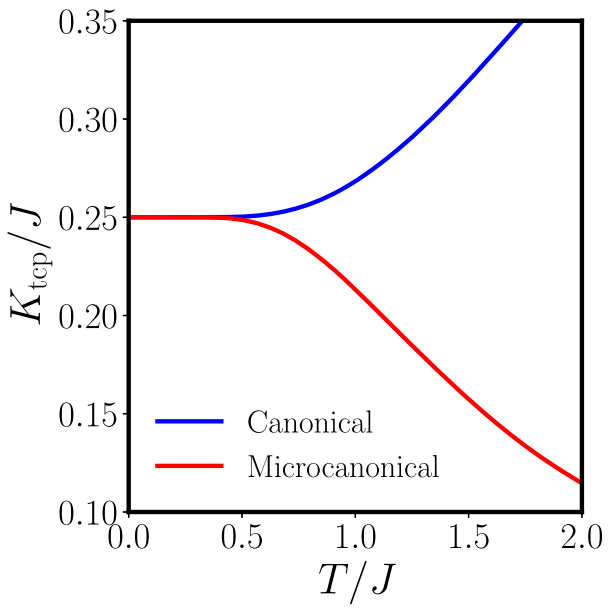

FIG. 3. The position of the trictitical point K/J against T/J in the canonical and microcanonical ensembles.

Inserting expression (37) in (34), the microcanonical ([MCE]) critical line becomes

$$h_c[\mathrm{MCE}] = 2J(1 - 2e^{-4\beta J}). \tag{38}$$

On the critical line, Eq. (35) becomes $J = 4Ks^2$, which yields the tricritical point at

$$K_{tcp}[\mathrm{MCE}] = J\left(\frac{1}{4} + e^{-4\beta J}\right). \tag{39}$$

When compared with the canonical analysis, this result presents an example of ensemble inequivalence. While the two ensembles lead to the same expression for the critical lines, (31), (38), they display distinct tricritical points. At a given temperature, the canonical tricritical point (32) is located at a lower value of K/J than the microcanonical one (39), [see Fig. 2 for the $(h/J, K/J)$ phase-diagram at a given low temperature]. In Fig. 3 we display the tricritical coupling K/J in the two ensembles, (32) and (39), as a function of T/J at low temperatures. While the tricritical points coincide at $T = 0$, the microcanonical one changes slower with temperature. Note that at any given temperature the magnetic field h/J at the tricritical point is the same in the two ensembles.

Conclusions—In this Letter, we studied the phase diagram of a model with long-range and multispin interactions, which exhibits a paramagnetic to ferromagnetic quantum phase transition at zero temperature. This transition has first-order and second-order branches separated by a tricritical point. At finite temperature, we showed that the model exhibits different phase diagrams in the canonical and microcanonical ensembles. While the two ensembles yield the same phase diagram at $T = 0$, they differ at finite temperatures. Notably, the position of the tricritical

point varies between the ensembles, with the finite temperature correction being larger in the canonical ensemble than in the microcanonical ensemble. Thus, the quantum tricritical points of long-range systems split due to finite temperature corrections, an effect that could not be predicted by the quantum-to-classical correspondence.

As AMO techniques continue to advance, our findings will become crucial to describe the critical scaling region of experimental platforms, where quantum fluctuations compete with long-range interactions. Indeed, while the Hamiltonian in Eq. (11) with $K = 0$ has already been employed in the description of cavity QED platforms [35,68,69], the realization of the four body term at $K > 0$ may be achieved by exploiting recent finding on cavity-mediated pair creation [70].

On general grounds, ensemble inequivalence is expected to occur whenever the canonical transition becomes first order in long-range quantum systems. Future investigations shall clarify how the phenomenon quantitatively arises in the case the first term in Hamiltonian (1) decays as a power-law of the distance $r^{-\alpha}$ with $\alpha < 1$.

Acknowledgments—Valuable discussions with G. Gori and A. Trombettoni are gratefully acknowledged. Relevant discussions on the experimental feasibility of our research with T. Donner are also acknowledged. This research was funded by the Swiss National Science Foundation (SNSF) Grant No. 200021 207537, by the Deutsche Forschungsgemeinschaft (DFG, German Research Foundation) under Germany's Excellence Strategy EXC2181/1-390900948 (the Heidelberg STRUCTURES Excellence Cluster), and the Swiss State Secretariat for Education, Research and Innovation (SERI). This work is part of MUR-PRIN2017 project "Coarse-grained description for non-equilibrium systems and transport phenomena (CONEST)" No. 201798CZL whose partial financial support is acknowledged. D. M. acknowledges the support of the Center for Scientific Excellence of the Weizmann Institute of Science. This research was supported in part by NSF Grants No. PHY-1748958 and No. PHY-2309135 to the Kavli Institute for Theoretical Physics (KITP).

[1] M. D. Lukin, Colloquium: Trapping and manipulating photon states in atomic ensembles, Rev. Mod. Phys. **75**, 457 (2003).

[2] M. Saffman, T. G. Walker, and K. Mølmer, Quantum information with Rydberg atoms, Rev. Mod. Phys. **82**, 2313 (2010).

[3] J. W. Britton, B. C. Sawyer, A. C. Keith, C. C. J. Wang, J. K. Freericks, H. Uys, M. J. Biercuk, and J. J. Bollinger, Engineered two-dimensional Ising interactions in a trapped-ion quantum simulator with hundreds of spins, Nature (London) **484**, 489 (2012).

[4] I. Bloch, J. Dalibard, and W. Zwerger, Many-body physics with ultracold gases, Rev. Mod. Phys. **80**, 885 (2008).

[5] R. Blatt and C. F. Roos, Quantum simulations with trapped ions, Nat. Phys. **8**, 277 (2012).

[6] C. Monroe, W. C. Campbell, L.-M. Duan, Z.-X. Gong, A. V. Gorshkov, P. W. Hess, R. Islam, K. Kim, N. M. Linke, G. Pagano, P. Richerme, C. Senko, and N. Y. Yao, Programmable quantum simulations of spin systems with trapped ions, Rev. Mod. Phys. **93**, 025001 (2021).

[7] F. Mivehvar, F. Piazza, T. Donner, and H. Ritsch, Cavity QED with quantum gases: New paradigms in many-body physics, Adv. Phys. **70**, 1 (2021).

[8] N. Defenu, T. Donner, T. Macrì, G. Pagano, S. Ruffo, and A. Trombettoni, Long-range interacting quantum systems, Rev. Mod. Phys. **95**, 035002 (2023).

[9] M. C. Angelini, G. Parisi, and F. Ricci-Tersenghi, Relations between short-range and long-range Ising models, Phys. Rev. E **89**, 062120 (2014).

[10] N. Defenu, A. Trombettoni, and A. Codello, Fixed-point structure and effective fractional dimensionality for O(N) models with long-range interactions, Phys. Rev. E **92**, 052113 (2015).

[11] N. Defenu, A. Trombettoni, and S. Ruffo, Anisotropic long-range spin systems, Phys. Rev. B **94**, 224411 (2016).

[12] N. Defenu, A. Trombettoni, and S. Ruffo, Criticality and phase diagram of quantum long-range O(N) models, Phys. Rev. B **96**, 104432 (2017).

[13] N. Defenu, A. Codello, S. Ruffo, and A. Trombettoni, Criticality of spin systems with weak long-range interactions, J. Phys. A Math. Gen. **53**, 143001 (2020).

[14] T. Dauxois, V. Latora, A. Rapisarda, S. Ruffo, and A. Torcini, *Dynamics and Thermodynamics of Systems with Long-Range Interactions*, edited by T. Dauxois, S. Ruffo, E. Arimondo, and M. Wilkens (Springer Berlin Heidelberg, Berlin, Heidelberg, 2002), pp. 458–487.

[15] A. Campa, T. Dauxois, and S. Ruffo, Statistical mechanics and dynamics of solvable models with long-range interactions, Phys. Rep. **480**, 57 (2009).

[16] A. Campa, T. Dauxois, D. Fanelli, and S. Ruffo, *Physics of Long-Range Interacting Systems* (Oxford University Press, New York, 2014).

[17] Y. Levin, R. Pakter, F. B. Rizzato, T. N. Teles, and F. P. Benetti, Nonequilibrium statistical mechanics of systems with long-range interactions, Phys. Rep. **535**, 1 (2014).

[18] J. Barré, D. Mukamel, and S. Ruffo, Inequivalence of ensembles in a system with long-range interactions, Phys. Rev. Lett. **87**, 030601 (2001).

[19] M. Kastner, Diverging equilibration times in long-range quantum spin models, Phys. Rev. Lett. **106**, 130601 (2011).

[20] S. Schütz and G. Morigi, Prethermalization of atoms due to photon-mediated long-range interactions, Phys. Rev. Lett. **113**, 203002 (2014).

[21] S. Schütz, S. B. Jäger, and G. Morigi, Dissipation-assisted prethermalization in long-range interacting atomic ensembles, Phys. Rev. Lett. **117**, 083001 (2016); T. Mori, Prethermalization in the transverse-field Ising chain with non-range interactions, J. Phys A: Math. Their. **52**, 054001 (2019).

[22] N. Defenu, Metastability and discrete spectrum of long-range systems, Proc. Natl. Acad. Sci. U.S.A. **118**, e2101785118 (2021).

[23] D. Mukamel, S. Ruffo, and N. Schreiber, Breaking of ergodicity and long relaxation times in systems with long-range interactions, Phys. Rev. Lett. **95**, 240604 (2005).
[24] F. Borgonovi, G. L. Celardo, M. Maianti, and E. Pedersoli, Broken ergodicity in classically chaotic spin systems, J. Stat. Phys. **116**, 1435 (2004).
[25] M. Kastner, Nonequivalence of ensembles for long-range quantum spin systems in optical lattices, Phys. Rev. Lett. **104**, 240403 (2010).
[26] M. Kastner, Nonequivalence of ensembles in the Curie-Weiss anisotropic quantum Heisenberg model, J. Stat. Mech. (2010) P07006.
[27] A. Russomanno, M. Fava, and M. Heyl, Quantum chaos and ensemble inequivalence of quantum long-range Ising chains, Phys. Rev. B **104**, 094309 (2021).
[28] L. Del Re, M. Fabrizio, and E. Tosatti, Nonequilibrium and nonhomogeneous phenomena around a first-order quantum phase transition, Phys. Rev. B **93**, 125131 (2016).
[29] D. S. Petrov, Elastic multibody interactions on a lattice, Phys. Rev. A **90**, 021601(R) (2014).
[30] A. Goban, R. B. Hutson, G. E. Marti, S. L. Campbell, M. A. Perlin, P. S. Julienne, J. P. D'Incao, A. M. Rey, and J. Ye, Emergence of multi-body interactions in a fermionic lattice clock, Nature (London) **563**, 369 (2018).
[31] W. Zwerger, Quantum-unbinding near a zero temperature liquid–gas transition, J. Stat. Mech. (2019) 103104.
[32] A. Griesmaier, J. Werner, S. Hensler, J. Stuhler, and T. Pfau, Bose-Einstein condensation of chromium, Phys. Rev. Lett. **94**, 160401 (2005).
[33] A. Micheli, G. K. Brennen, and P. Zoller, A toolbox for lattice-spin models with polar molecules, Nat. Phys. **2**, 341 (2006).
[34] K.-K. Ni, S. Ospelkaus, M. H. G. de Miranda, A. Pe'er, B. Neyenhuis, J. J. Zirbel, S. Kotochigova, P. S. Julienne, D. S. Jin, and J. Ye, A high phase-space-density gas of polar molecules, Science **322**, 231 (2008).
[35] S. Morrison and A. S. Parkins, Dynamical quantum phase transitions in the dissipative Lipkin-Meshkov-Glick model with proposed realization in optical cavity QED, Phys. Rev. Lett. **100**, 040403 (2008).
[36] J. Larson, Circuit QED scheme for the realization of the Lipkin-Meshkov-Glick model, Europhys. Lett. **90**, 54001 (2010).
[37] T. Keller, V. Torggler, S. B. Jäger, S. Schütz, H. Ritsch, and G. Morigi, Quenches across the self-organization transition in multimode cavities, New J. Phys. **20**, 025004 (2018).
[38] Z. Wu, J. Fan, X. Zhang, J. Qi, and H. Wu, Signatures of prethermalization in a quenched cavity-mediated long-range interacting Fermi gas, Phys. Rev. Lett. **131**, 243401 (2023).
[39] T. Albash and D. A. Lidar, Adiabatic quantum computation, Rev. Mod. Phys. **90**, 015002 (2018).
[40] H. J. Lipkin, N. Meshkov, and A. J. Glick, Validity of many-body approximation methods for a solvable model, Nucl. Phys. **62**, 188 (1965).
[41] N. Meshkov, A. J. Glick, and H. J. Lipkin, Validity of many-body approximation methods for a solvable model. (II). Linearization procedures, Nucl. Phys. **62**, 199 (1965).
[42] A. J. Glick, H. J. Lipkin, and N. Meshkov, Validity of many-body approximation methods for a solvable model. (III). Diagram summations, Nucl. Phys. **62**, 211 (1965).
[43] R. H. Dicke, Coherence in spontaneous radiation processes, Phys. Rev. **93**, 99 (1954).
[44] K. Baumann, C. Guerlin, F. Brennecke, and T. Esslinger, Dicke quantum phase transition with a superfluid gas in an optical cavity, Nature (London) **464**, 1301 (2010).
[45] R. Landig, F. Brennecke, R. Mottl, T. Donner, and T. Esslinger, Measuring the dynamic structure factor of a quantum gas undergoing a structural phase transition, Nat. Commun. **6**, 7046 (2015).
[46] J. Reslen, L. Quiroga, and N. F. Johnson, Direct equivalence between quantum phase transition phenomena in radiation-matter and magnetic systems: Scaling of entanglement, Europhys. Lett. **69**, 8 (2005).
[47] S. Schütz, S. B. Jäger, and G. Morigi, Thermodynamics and dynamics of atomic self-organization in an optical cavity, Phys. Rev. A **92**, 063808 (2015).
[48] I. D. Leroux, M. H. Schleier-Smith, and V. Vuletić, Implementation of cavity squeezing of a collective atomic spin, Phys. Rev. Lett. **104**, 073602 (2010).
[49] G. Bentsen, I.-D. Potirniche, V. B. Bulchandani, T. Scaffidi, X. Cao, X.-L. Qi, M. Schleier-Smith, and E. Altman, Integrable and chaotic dynamics of spins coupled to an optical cavity, Phys. Rev. X **9**, 041011 (2019).
[50] E. J. Davis, G. Bentsen, L. Homeier, T. Li, and M. H. Schleier-Smith, Photon-mediated spin-exchange dynamics of spin-1 atoms, Phys. Rev. Lett. **122**, 010405 (2019).
[51] E. J. Davis, A. Periwal, E. S. Cooper, G. Bentsen, S. J. Evered, K. Van Kirk, and M. H. Schleier-Smith, Protecting spin coherence in a tunable Heisenberg model, Phys. Rev. Lett. **125**, 060402 (2020).
[52] A. Gallemí, G. Queraltó, M. Guilleumas, R. Mayol, and A. Sanpera, Quantum spin models with mesoscopic Bose-Einstein condensates, Phys. Rev. A **94**, 063626 (2016).
[53] T.-L. Ho, Spinor bose condensates in optical traps, Phys. Rev. Lett. **81**, 742 (1998).
[54] T. Ohmi and K. Machida, Bose-Einstein condensation with internal degrees of freedom in alkali atom gases, J. Phys. Soc. Jpn. **67**, 1822 (1998).
[55] J. Stenger, S. Inouye, D. M. Stamper-Kurn, H. J. Miesner, A. P. Chikkatur, and W. Ketterle, Spin domains in ground-state Bose-Einstein condensates, Nature (London) **396**, 345 (1998).
[56] M.-S. Chang, C. D. Hamley, M. D. Barrett, J. A. Sauer, K. M. Fortier, W. Zhang, L. You, and M. S. Chapman, Observation of spinor dynamics in optically trapped ^{87}Rb Bose-Einstein condensates, Phys. Rev. Lett. **92**, 140403 (2004).
[57] H. Schmaljohann, M. Erhard, J. Kronjäger, M. Kottke, S. van Staa, L. Cacciapuoti, J. J. Arlt, K. Bongs, and K. Sengstock, Dynamics of $f = 2$ spinor Bose-Einstein condensates, Phys. Rev. Lett. **92**, 040402 (2004).
[58] T. M. Hoang, M. Anquez, B. A. Robbins, X. Y. Yang, B. J. Land, C. D. Hamley, and M. S. Chapman, Parametric excitation and squeezing in a many-body spinor condensate, Nat. Commun. **7**, 11233 (2016).

[59] H. Weimer, M. Müller, I. Lesanovsky, P. Zoller, and H. P. Büchler, A Rydberg quantum simulator, Nat. Phys. **6**, 382 (2010).

[60] N. Henkel, R. Nath, and T. Pohl, Three-dimensional roton excitations and supersolid formation in Rydberg-excited Bose-Einstein condensates, Phys. Rev. Lett. **104**, 195302 (2010).

[61] L. I. R. Gil, R. Mukherjee, E. M. Bridge, M. P. A. Jones, and T. Pohl, Spin squeezing in a Rydberg lattice clock, Phys. Rev. Lett. **112**, 103601 (2014).

[62] J. Zeiher, P. Schauß, S. Hild, T. Macrì, I. Bloch, and C. Gross, Microscopic characterization of scalable coherent Rydberg superatoms, Phys. Rev. X **5**, 031015 (2015).

[63] Y. Y. Jau, A. M. Hankin, T. Keating, I. H. Deutsch, and G. W. Biedermann, Entangling atomic spins with a Rydberg-dressed spin-flip blockade, Nat. Phys. **12**, 71 (2016).

[64] S. Will, T. Best, U. Schneider, L. Hackermüller, D.-S. Lühmann, and I. Bloch, Time-resolved observation of coherent multi-body interactions in quantum phase revivals, Nature (London) **465**, 197 (2010).

[65] H. P. Büchler, A. Micheli, and P. Zoller, Three-body interactions with cold polar molecules, Nat. Phys. **3**, 726 (2007).

[66] E. H. Lieb, The classical limit of quantum spin systems, Commun. Math. Phys. **31**, 327 (1973).

[67] E. Granet, Exact mean-field solution of a spin chain with short-range and long-range interactions, SciPost Phys. **14**, 133 (2023).

[68] S. Morrison and A. S. Parkins, Collective spin systems in dispersive optical cavity QED: Quantum phase transitions and entanglement, Phys. Rev. A **77**, 043810 (2008).

[69] J. G. Cosme, J. Skulte, and L. Mathey, Bridging closed and dissipative discrete time crystals in spin systems with infinite-range interactions, Phys. Rev. B **108**, 024302 (2023).

[70] F. Finger, R. Rosa-Medina, N. Reiter, P. Christodoulou, T. Donner, and T. Esslinger, Spin- and momentum-correlated atom pairs mediated by photon exchange and seeded by vacuum fluctuations, Phys. Rev. Lett. **132**, 093402 (2024).